Submicron drops from flapping bursting bubbles

Xinghua Jiang[a,1], Lucas Rotily[b], Emmanuel Villermaux[b,c,1], and Xiaofei Wang[a,d,e,1,2]

[a]Department of Environmental Science and Engineering, Shanghai Key Laboratory of Atmospheric Particle Pollution and Prevention, Fudan University, Shanghai 200433, China; [b]Institut de Recherche sur les Phénomènes Hors Equilibre, Aix-Marseille Université, Marseille CEDEX 13 13384, France; [c]Institut Universitaire de France, Paris 75005, France; [d]Shanghai Institute of Pollution Control and Ecological Security, Shanghai 200092, China; and [e]Cluster of Interfacial Processes Against Pollution, Fudan University, Shanghai 200433, China

Edited by David Weitz, Department of Physics, Division of Engineering and Applied Science, Harvard University, Cambridge, MA; received July 14, 2021; accepted November 30, 2021

Tiny water drops produced from bubble bursting play a critical role in forming clouds, scattering sunlight, and transporting pathogens from water to the air. Bubbles burst by nucleating a hole at their cap foot and may produce jets or film drops. The latter originate from the fragmentation of liquid ligaments formed by the centripetal destabilization of the opening hole rim. They constitute a major fraction of the aerosols produced from bubbles with cap radius of curvature (R) > ∼0.4 × capillary length (a). However, our present understanding of the corresponding mechanisms does not explain the production of most submicron film drops, which represent the main number fraction of sea spray aerosols. In this study, we report observations showing that bursting bubbles with $R < \sim 0.4a$ are actually mainly responsible for submicron film drop production, through a mechanism involving the flapping shear instability of the cap with the outer environment. With this proposed pathway, the complex relations between bubble size and number of drops produced per bubble can be better explained, providing a fundamental framework for understanding the production flux of aerosols and the transfer of substances mediated by bubble bursting through the air–water interface and the sensitivity of the process to the nature of the environment.

film drop | bubble | flapping

Bubble bursting is a fundamentally important physical process in nature, which has crucial environmental and climate ramifications (1–12). Wave breaking over the oceans produces large amounts of bubbles, which eventually burst and eject water drops known as sea spray aerosols. These spray aerosols mediate the transfer of moisture, salts, organics, and microorganisms through the water–air interface and exert significant effects on atmospheric chemistry (4, 13), human health and climate (4, 13–17). Our current understanding of surface bubble bursting aerosol formation includes two major pathways, namely film drop (5) and jet drop production (6) (Fig. 1*A*). When a bubble reaches the water surface, its film cap thins until a hole nucleates close to its foot. Then, the rim of the hole expands at the Taylor-Culick velocity ($v = \sqrt{\frac{2\sigma}{\rho_1 h}}$, where ρ_1 is the density of the liquid phase, σ is its surface tension, and h is bubble cap film thickness). The receding rim follows the curvature of the film cap, thereby experiencing a centripetal acceleration, which suffers a Rayleigh-Taylor instability and produces multiple liquid ligaments. Then, these ligaments further break into droplets, commonly known as film drops (6, 7, 18, 19). The collapse of the remaining bubble cavity forms a Worthington upward jet, which may also break into multiple drops, known as jet drops (7, 8, 20, 21).

Many studies (1, 9, 10, 15) have investigated the size distributions of bubble bursting drops confirming that submicron drops are the dominant fraction of the total number of drops produced, and they usually peak at ∼100 to 200 nm. By submicron drop, we mean a drop with a dried diameter less than 1 μm. In sea spray aerosols, this dried diameter (D_p; see *Methods* for the detailed description) is roughly 1/4 of the original drop diameter, since the salinity of seawater is usually ∼3.5% (4, 8, 22). However, the current understanding of the processes at play cannot fully explain the origin of these submicron drops. Based on the relation between the sizes of jet drops and their parent bubbles, only sub–100-μm bubbles can produce submicron jet drops (23–27). Our previous work demonstrates that jet drops usually account for ∼20 to 40% of submicron sea spray aerosols (13, 20). The remaining 60 to 80% of submicron sea spray aerosols should originate from the fragmentation of the bubble caps, named film drops. However, bubbles with cap radii of curvature $R > \sim 0.4a$ produce film drops (7) with an average drop diameter $\langle d \rangle$ such that

$$\langle d \rangle \sim R^{3/8} h^{5/8}, \quad [1]$$

with $h \sim \frac{R^2}{\mathcal{L}}$ the bubble cap thickness, $\mathcal{L} = \beta a$ with $a = \sqrt{\frac{2\sigma}{\rho_1 g}}$ the capillary length and β is $O(10^3)$, a relation valid for $R > \sim 1$ mm. For pure water and seawater, a is ∼2.7 mm. Thus, the smallest typical film drop diameters $\langle d \rangle$ formed that way are O(7 μm), giving a dried diameter O(2 μm), appreciably larger than the submicron bubble bursting aerosols, which usually have a dry diameter around 100 to 200 nm.

The above centrifuge theory for $\langle d \rangle$ of film drops is consistent with previous experimental investigations from Lhuissier and Villermaux (7). However, it cannot explain the production of film drops from bubbles with $R < \sim 0.4a$ (∼1 mm for water), as some other experiments show that millimetric bubbles do produce many submicron drops, which are likely to be film drops (28). Critical questions thus arise: Why can bubbles with $R < \sim 0.4a$ (∼1 mm for water) produce film drops? What is the mechanism?

Significance

Bubble bursting aerosols play a critical role in forming clouds, scattering sunlight, and transporting pathogens from water to the air. Most of them are produced from the fragmentation of bubble cap film. They usually have a diameter below 1 μm. However, their physical production mechanism has remained unknown. In this work, we discovered that these drops are probably generated from flapping bubble cap film (like a flapping flag). It explains the mysterious relation between bubble size and number of drops produced per bubble, providing a fundamental framework for understanding the production flux of bubble bursting aerosols, such as sea spray aerosol, and substance transfer through the air–water interface during drop ejection.

Author contributions: E.V. and X.W. designed research; X.J., L.R., E.V., and X.W. performed research; X.J., E.V., and X.W. analyzed data; and X.J., E.V., and X.W. wrote the paper.

The authors declare no competing interest.

This article is a PNAS Direct Submission.

This article is distributed under Creative Commons Attribution-NonCommercial-NoDerivatives License 4.0 (CC BY-NC-ND).

[1]X.J., E.V., and X.W. contributed equally to this work.

[2]To whom correspondence may be addressed. Email: xiaofeiwang@fudan.edu.cn.

This article contains supporting information online at http://www.pnas.org/lookup/suppl/doi:10.1073/pnas.2112924119/-/DCSupplemental.

Published December 30, 2021.

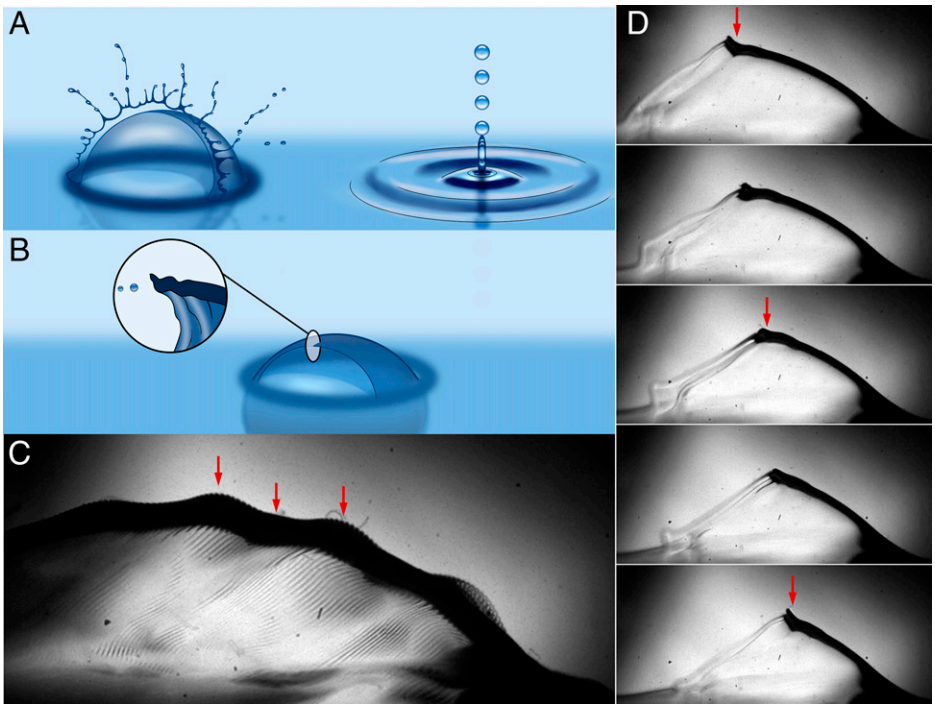

Fig. 1. Conventional and observed mechanisms for bubble bursting drop production. (*A*) Conventional view of bubble bursting drop production, including film drop production from the centripetal acceleration and jet drop production from the collapse of bubble cavity; (*B*) flapping mechanism of a recessing bubble cap film: the interaction between fast-moving water film and its surrounding gas; (*C*) picture of bursting of an FC43 (perfluorotributylamine) bubble with an $R = 3.2$ mm in water; (*D*) successive pictures of this bubble bursting process. The time between each frame is 6/20,000 s.

In this study, we report film drop production from bursting of bubbles with various radius in different gas environment. With the measured characteristics of these film drops and visualization of bubble bursting process, a comprehensive theory on bubble bursting film drop generation is proposed.

Results and Discussion

Submicron Film Drop Production from Bubbles with $R < \sim 0.4a$. In order to improve smaller size detection, we use here a scanning mobility particle sizer (SMPS) and an aerodynamic particle sizer (APS) to obtain the size distributions of aerosols from bubbles bursting at the surface of a pool. Fig. 2 (and *SI Appendix*, Fig. S2) clearly shows that bubbles with radius R of 73 to 1,080 μm did produce a dominant number fraction of submicron drops from a 3.5% NaCl water solution and seawater (see *Methods* for the details about its sampling information). The size of these submicron drops peak at ~30 to 100 nm. These drops must be film drops, since the dry diameters of jet drops produced from the bubbles with $R = 73$, 137, 199, 870, and 1,080 μm are 0.28, 0.62, 1.0, 6.8, and 9.2 μm, respectively, based on the relation between jet drop size and bubble size compiled by Berny et al. (23). These jet drop sizes are significantly larger than the sizes shown in Fig. 2. In addition, a cascade of small daughter bubbles could form after the bursting of a large bubble (29). It is unlikely that these daughter bubbles play a significant role in submicron drop production from these bubbles with $R < \sim 0.4a$. In air, Bird et al. report that the average daughter bubble size is roughly 0.08 times of the parent bubble size (29). If the bubbles with $R = 73$, 137, 199, 870, and 1,080 μm do produce daughter bubbles, their bubbles' R would be 5.8, 11.0, 15.9, 69.6, and 86.4 μm. Based on the relation compiled by Berny et al., the dried sizes of jet drops from these daughter bubbles would be 24, 52, 83, 532, and 700 nm, which are inconsistent from the size distributions shown in Fig. 2. Finally, the existence of these film drops is also inconsistent with the centrifuge film drop production mechanism (6, 7), which requires that $R > \sim 0.4a$, suggesting that a missing film drop production mechanism operating on smaller bubbles.

Proposed Theory of Film Drop Production. Any liquid drop originates from the fragmentation of a ligament, which should be produced by some instability. The conventional view is that, just after hole nucleation, the fast-moving rim experiences a centrifuge Rayleigh-Taylor instability along the curved bubble cap with a growth rate (7)

$$t_{RT}^{-1} \sim \sqrt{\frac{\sigma}{\rho_1 (Rh)^{3/2}}}. \qquad [2]$$

For instability to have an appreciable gain, the rim recession time over the bubble cap T should be larger than t_{RT}, thus requiring $Tt_{RT}^{-1} > 1$. The bubble cap extent is $E \sim \frac{R^2}{a}$ for $R < a$, and the rim travels at the Taylor-Culick velocity so that $T = E/v$. For this centrifuge instability to onset, bubbles should thus be sufficiently large since

$$t_{RT}^{-1} T \sim \frac{\beta^{\frac{1}{4}} \left(\frac{R}{a}\right)^{\frac{3}{4}}}{\sqrt{2}} > 1 \qquad [3]$$

implies that $R/a > \sim (4^{-1}\beta)^{-1/3}$. Smaller bubbles have too short a residence time to grow such an instability.

However, bubbles with a smaller radius also have a smaller thickness and therefore a faster hole receding speed. Previous observations have shown that receding thin films, like soap films, are light enough to be sensitive to their environment (30) and flap like flags do in the wind, suffering a shear instability, named after Squire in this context (31). Is it strong enough to destabilize small bubbles' cap films? To probe this question, we compare as before the rim recession time T with the Squire instability growth rate (31, 32)

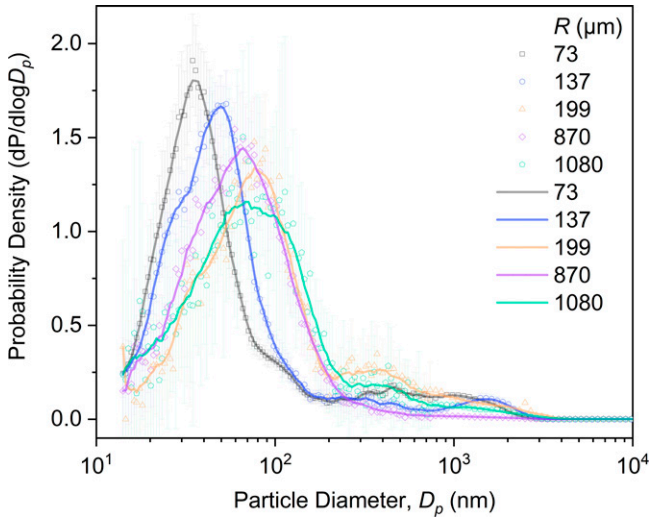

Fig. 2. Particle size distributions of bubble bursting drops (dried) in terms of probability (P) density function. Drops are produced from the bubbles with various R from salt water (3.5% sodium chloride solution) at the air–water interface. The curves are smoothed by using the adjacent average method.

$$t_S^{-1} = \frac{\rho_2}{\rho_1}\frac{v}{h}, \qquad [4]$$

where ρ_2 is the density of the surrounding gas. The condition for the onset of the flapping instability is again $Tt_S^{-1} > 1$, a criterion that translates into $\frac{\rho_2}{\rho_1}\frac{\mathcal{L}}{a} > 1$, or

$$\frac{\rho_2}{\rho_1} > \frac{1}{\beta}. \qquad [5]$$

For a water–air interface with $\rho_1 = 10^3$ kg · m^{-3} and $\rho_2 = 1.2$ kg · m^{-3}, we see that the above criterion predicts interestingly that this instability is possible but is close to marginal and that increasing appreciably the density of the gas phase should reveal more clearly its existence.

As summarized in Fig. 3*A* (or *SI Appendix*, Fig. S3), the above elements predict that 1) large bubbles $[R/a > \sim(4^{-1}\beta)^{-1/3}]$ destabilize via a centrifuge Rayleigh-Taylor instability; 2) small bubbles $[R/a < \sim(4^{-1}\beta)^{-1/3}]$ must be in a dense gas environment $(\rho_2/\rho_1 > \beta^{-1})$ to flap via a Squire instability, as illustrated in Figs. 1*B*; and 3) there are two distinct modes of film drop production, with different features depending on bubble size and environment density.

Experimental Verification of the Predictions from the Proposed Theory. Prediction 1 has already been convincingly demonstrated (7). To test prediction 2, we recorded small bursting bubbles under a microscope, at 200,000 frame rate per second. Indeed, the corresponding busting sequence is quick (T is a fraction of a milliseconds for a millimetric bubble) and the anticipated outcome aerosols a size on the order of or smaller than the wavelength of light. *SI Appendix*, Figs. S4 and S5 show the bursting of small single bubbles with $R = 0.87$ to 1.25 mm at a water–air $\left(\frac{\rho_2}{\rho_1} = \frac{1.2}{1{,}000} \sim \beta^{-1}\right)$ or water–sulfur hexafluoride (SF_6) interface $\left(\frac{\rho_2}{\rho_1} = \frac{7}{1{,}000} > \beta^{-1}\right)$. As expected, no long-centrifuged ligaments are found since the standard Rayleigh-Taylor instability has no sufficient time to amplify. However, it is found that the bursting of an $R = 0.87$ mm and an $R = 1.25$ mm SF_6 water bubble in an SF_6 environment does produce drops (*SI Appendix*, Fig. S4). The drops fly horizontally, suggesting that another instability, such as Squire instability, responsible for their formation has just developed at the end of the rim travel along the bubble cap. Unfortunately, the flapping motion is hardly discerned because of time and space resolution limitations.

To overcome this technical difficulty, we conducted an analog experiment by bursting a larger $R = 3.2$ mm perfluorotributylamine

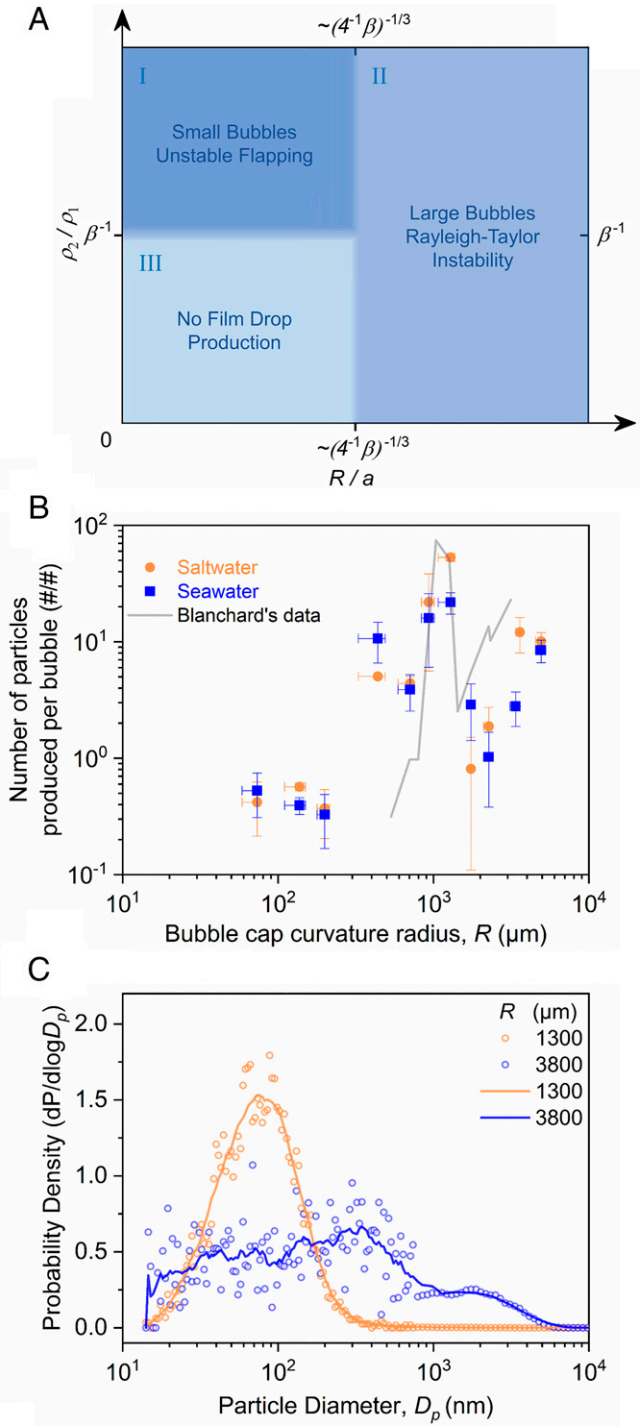

Fig. 3. Characteristics of submicron drops produced from bursting of bubbles at the air–water interface. (*A*) Diagrams of the regimes for 1) Squire (flapping) instability $\left[\frac{\rho_2}{\rho_1} > \frac{1}{\beta}\right.$ and $\left.R/a < \sim(4^{-1}\beta)^{-1/3}\right]$, 2) Rayleigh-Taylor instability, and 3) no film drop production; (*B*) number of submicron drops produced per bubble with a range of bubble sizes. The error bars in bubble sizes were derived from the abscissa of the cumulative frequency of ~25 to 75% in the frequency distribution diagram (*SI Appendix*, Figs. S10–S12). (*C*) Particle number size distributions of dried drops produced from the bursting of bubbles with R = 1,300 or 3,800 μm.

(FC43) bubble into water. The density ratio $\frac{\rho_2}{\rho_1} = \frac{1,000}{1,884}$ is much larger than for a water–gas couple, so the Rayleigh-Taylor centrifuge instability grows much more slowly in this case, allowing more time for the flapping motion to set in. Screening the Rayleigh-Taylor mechanism by matching the densities and using larger bubbles allows us to focus on the anticipated shear mechanism, which is then clearly observed: The bursting sequence (Fig. 1*C* and Movie S1) does show a flapping receding bubble cap. In addition, Movies S2 and S3 also show film fragmentation and drop formation from the flapping bubble cap. The flapping bursting mode thus does onset when it is expected to.

To test prediction 3, we measured the number of submicron drops produced per bubble n according to their size R from salt water (3.5% NaCl) and seawater (Fig. 3*B* and *SI Appendix*, Fig. S6). As expected, a distinct transition between the ranges of small and large bubble sizes is observed, which are separated by a significant dip at $R \approx 1$ to 2 mm $\sim(4^{-1}\beta)^{-1/3}a$. Obviously, this sharp transition reflects the two film drop production mechanisms, supporting our discussion above: Flapping and centrifuge mechanisms are responsible for film drop production when $R < \sim(4^{-1}\beta)^{-1/3}a$ and $R > \sim(4^{-1}\beta)^{-1/3}a$, respectively. The present investigation is also a clue for the long-standing puzzle posed by Blanchard and Syzdek's study, reporting the until-now unexplained existence of a large peak in the drop production histogram for bubble diameters of order 2 to 2.5 mm with a maximum n of ~80 drops per bubble (28, 33), producing drops with sizes below 300 nm (33, 34).

Fig. 3*B* also shows that the large bubbles $[R > \sim(4^{-1}\beta)^{-1/3}a]$ produce submicron drops and the production rate decreases exponentially with bubble size decreasing to $\sim(4^{-1}\beta)^{-1/3}a$, at which it is shut down. Their production is likely to associate with the centrifuge film drops, as the number of centrifuge drops also decrease with bubbles sizes decrease, and the production of the centrifuge drops are also shut down when R is $\sim(4^{-1}\beta)^{-1/3}a$. Thus, based on this concurrence, it is proposed that these drops might be the satellite drops produced around the centrifuge drops.

Differences in Sizes Between the Two Film Drop Production Pathways. The film drop production from between bubbles with $R > \sim(4^{-1}\beta)^{-1/3}a$ and $R < \sim(4^{-1}\beta)^{-1/3}a$ have a distinct difference in their size distributions. Fig. 3*C* shows that the small bubbles with $R = 1{,}300\ \mu m < \sim(4^{-1}\beta)^{-1/3}a$ have a significant size peak over the submicron range, while the large bubbles with $R = 3{,}800\ \mu m > \sim(4^{-1}\beta)^{-1/3}a$ have an almost flat size distribution over the entire $\sim 10^1$ to 10^3 nm size range.

Film Drop Production in Different Gas Environments. Prediction 3 also implies that the film drop production rate is affected by the gas density, especially for smaller bubbles. Fig. 4 shows the particle diameter distributions of dried drops produced by bursting small bubbles in air, SF_6, and He with densities of 1.2, 6.1, and 0.16 kg/m^3, respectively. The volumetric injection gas flow rates were kept constants for all these experiments. The denser SF_6 environment presents remarkably the largest film drop production rate, while the lighter He has the smallest drop production rate, demonstrating that the gas density does play a critical role in film drop production.

Tlhe average drops sizes produced by the flapping mechanism (31) is $\langle d \rangle \sim \sqrt{vt_s h} \sim h\sqrt{\frac{\rho_1}{\rho_2}}$, corresponding to d ~300 nm for $R = 100\ \mu m$ in air, giving a dried particle size somewhat smaller than 100 nm, consistently with Fig. 4 and *SI Appendix*, Fig. S7. Their maximal number per bubble burst is expected to be on the order of $n_{max} \sim \left(\frac{R^2}{a}\right)^2 \frac{h}{d^3} \sim \beta^2 \left(\frac{\rho_2}{\rho_1}\right)^{\frac{3}{2}}$, assuming all film cap material forms drops, so that n_{max} ~30 in air. However, it is important to point out that this n_{max} does not capture possible satellite drop formation around the primary flapping drops. Thus, the current theory cannot predict the exact number of film drops produced per bubble.

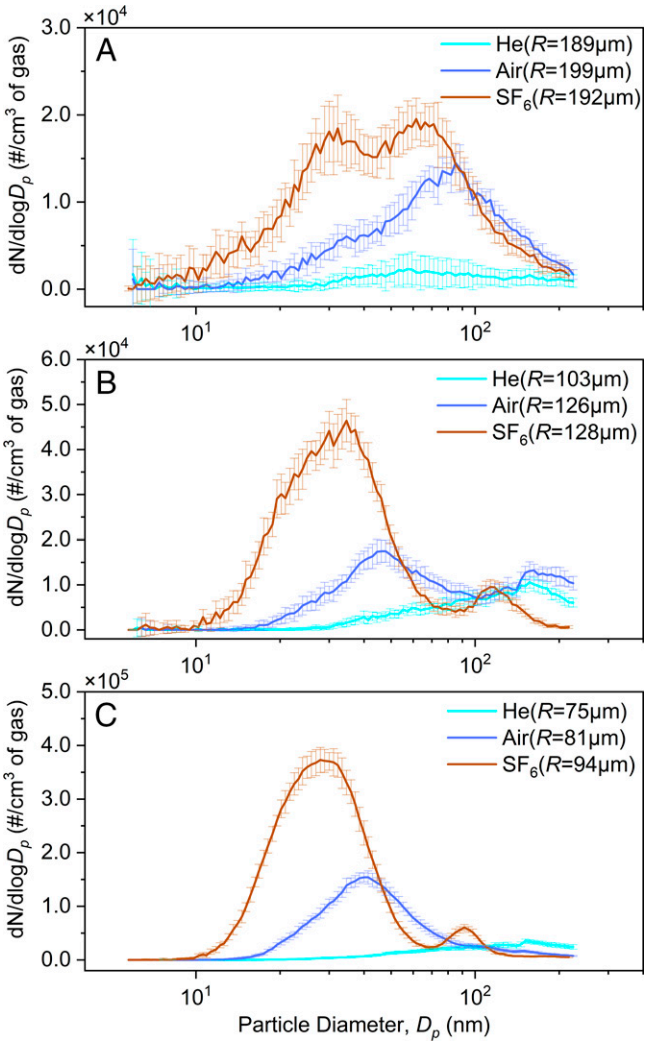

Fig. 4. Particle size distributions of bubble bursting drops (dried) in different gas environments for (*A*) bubbles with R = ~200 μm; (*B*) bubbles with R = ~120 μm; and (*C*) bubbles with R = ~80 μm. N is the number concentration of drops in each gas.

We also measured the size distribution for dried drops produced from bursting of even smaller bubbles with an $R \approx 40\ \mu m$ in the salt solution (*SI Appendix*, Fig. S8), which is distinct from the drop size distributions from the bursting of bubbles in Fig. 2. The main peak at ~500 nm must originate from the jet drop production mechanism since the location of this peak follows the relation between the sizes of jet drops and their parent bubbles (23). Very few film drops are produced, indicating that this mechanism is shut down at this bubble size, thus suggesting that the lower bubble size limit for film drop production should be in the range of 40 to 60 μm.

Atmospheric Implications. Together with the centripetal acceleration mechanism, the newly found flapping mechanism establishes a general framework to explain submicron film drop production. Combining the n versus R relation in Fig. 3*B* with the measured bubble size distribution (8, 35) from wave breaking in ocean water, one can infer a probability density function for film drops produced at each bubble size R (*SI Appendix*, Fig. S9), showing that the bubbles with $R < \sim 1$ mm produce a main number fraction of submicron film drops through the pathway from flapping films.

It is well known that smaller sea spray aerosol would contain more organics. For example, sub–100-nm sea spray aerosols usually have an organic content higher than 50% (36), which still do not have a theory to explain. Surface active organics would form a single molecular layer on the air–water interfaces, including both the inner and outer sides of the bubble cap film. The surface concentrations of organics are determined by their concentrations in bulk, following the Langmuir adsorption equilibrium (37, 38). With the knowledge of bubble cap film thickness and bubble cap size, the mass of water in the bubble cap is known, and the organic mass fraction of the cap film can be calculated. Obviously, thinner film thickness results in higher organic fraction. Assuming the composition of film drop is equal to the cap film, the organic fraction of film drop is obtained.

The centrifuge mechanism only allows film drop produced from bubbles with $R > \sim 1$ mm. The bubble cap thickness would be larger than 100 nm for these bubbles (7). For a typical concentration of organics on seawater surface (0.1 to 1 mg/m^2) (37), the organic mass fraction of film drops produced from these large bubbles is very unlikely to be larger than 50%.

In contrast, the flapping mechanism allows film drop produced from submillimeter bubbles, the bubble caps of which are much thinner. For example, the cap thickness of a bubble with $R = 0.5$ mm is ~10 nm (7). The organic fractions of the film drops would be easily larger than 50%, thereby explaining the observation of the high organic mass fraction for sub–100-nm sea spray aerosols.

Natural water such as seawater is a complex mixture containing tens of thousands of chemical species, debris, and many microorganisms, all of them susceptible to being transferred aloft in air by bubble bursting. Knowing the detailed production mechanisms and associated aerosol size ranges is critical to understand the chemical and biological compositions thus produced. We have shown here that these are all film drops, the smallest being mediated by a flapping mechanism sensitive to the environment. This will help to better describe the transfer of momentum, heat, and organic and inorganic substances through the water–air interface (4, 7, 13) and to understand the role played by the environment on these phenomena.

Methods

Salt Water and Seawater. The 3.5% sodium chloride solution is made from ultrapure water with a resistivity of 18 MΩ · cm and NaCl (analytically pure, China National Pharmaceutical Group Co., Ltd.). All the seawater used in this study is collected from the Yellow Sea (36°N:124°E). After standing for several hours, we remove the sediment and store the seawater in a refrigerator.

Experimental Setup. The setup is shown in *SI Appendix*, Fig. S1. The gas is pushed through a high-efficiency particulate arrestance (HEPA) filter with a certain flow. Then it splits into two streams, both of which are controlled by mass flow controllers. One stream passes through a glass filter or a needle to produce bubbles with various sizes. Another stream enters the water tank directly with a constant flow rate (*SI Appendix*, Tables S1 and S2) to bring bubble bursting drops out of the tank. Before any aerosol measurements, the silica diffusion dryer is used to dry drops to form solid aerosol particles. To make sure there is no contaminated aerosol in the system, the particle free gas is used to purge the whole system until the particle concentration is zero (<0.01 particle/cm^3). The particle concentration is measured by a condensational particle counter (CPC) (Model 3775, TSI Inc.).

Definition of D_p. Particle size is usually defined by its measuring method. Here, size distributions of dried bubble bursting drops are measured by two instruments: an SMPS and an APS (Model 3321, TSI Inc.). The SMPS consists of two components, a differential mobility analyzer (Model 3081, TSI Inc.) and a CPC (Model 3775, TSI Inc.). The size ranges for the SMPS and APS are ~7 to 700 nm and ~500 to 20,000 nm, respectively. SMPS can measure electrical mobility particle diameter (D_m), while APS can measure aerodynamic particle diameter (D_a). These two diameters are different and have the following relation (39):

$$D_m = D_a \sqrt{\chi^3 \frac{\rho_0}{\rho_p}}, \quad [6]$$

where χ is dynamic shape factor under the ambient condition, ρ_p is the particle density, and ρ_0 is the reference density (1 g/cm^3). In this paper, we define particle diameter, D_p, as D_m.

The drop production mechanism from fresh water would be expected to be similar to salt water, as the differences in surface tension, density, and viscosity between these two waters are actually small. However, the water drop would dry quickly in ambient air with low humidity. Fresh water has much fewer numbers of residues. Thus, the size of these dried aerosols would be much smaller than those particles produced from 3.5% salt water.

Experiments for Studying the Particle Size Distributions of Bubble Bursting Drops. The numbers of bubbles used for calculating each curve in Fig. 2 are ~9.7×10^8, 1.5×10^8, 4.8×10^7, 2.0×10^6, and 9.6×10^5, and the numbers of drops collected are ~1.3×10^8, 6.1×10^7, 5.7×10^6, 8.2×10^6, and 1.5×10^6 for bubbles' $R = 73$, 137, 199, 870, and 1,080 μm.

The number production rate of bubbles produced through the frits are measured to be 4.04×10^5, 6.15×10^4, 2.01×10^4, 8.22×10^2, and 3.98×10^2 per second for bubbles' $R = 73$, 137, 199, 870, and 1,080 μm, respectively. Then, the particle size distributions in Fig. 2 are measured. The sampling time of each measurement is 240 s. Every curve in Fig. 2 is averaged by ~10 sets of measurements. Therefore, the total number of bubbles during each measurement is just the number production rate of bubbles times the sampling time (~2,400 s). Moreover, the air sampling flow rate is 0.3 liter per minute (LPM). Thus, the total number of drops that are sampled is the drop concentration in the air times air sampling flow rate times the sampling time.

Measurement of Bubble Size. Bubble sizes are measured by a microscopic camera (Model TipScope CAM, TipScope Inc.) or a regular camera (Model RX10, Sony Corp.) depending on their sizes. For smaller bubbles ($R < 400$ μm), their shapes in water remain spherical. Thus, the microscopic camera with an extremely narrow depth of focus is used to take pictures of bubbles. By comparing the diameter of the bubbles that are in focus to a scale, bubble diameter can be obtained. For large bubbles ($R > 400$ μm), their shapes are not spherical in water. Thus, we use a camera to take pictures of these bubbles on water surface. The maximum horizontal radius of the bubble can be converted to the volume equivalent radius based on Toba (1959) (40). The values of the error bar of the bubble particle size measurement are the abscissa values corresponding to 25 to 75% of the cumulative frequency of the measured value frequency distribution graph (*SI Appendix*, Figs. S10–S12).

Gas Dilution for CPC Measurement. CPC measurement could be affected when pure He or SF_6 were directly used as the carrier gas for particles (41). A solution is found and tested: When these gases are diluted with air with the dilution ratio >6:1, then the CPC measurement is not affected. Therefore, a dilution ratio of 9:1 is used for all the gas density experiments.

Setup for Bubble Visualizations. The setup for the bubbles visualizations includes a tank filled with water and a ceiling filled with either air or SF_6. Backlighting plus microscope lens are used for capturing high-speed pictures.

Data Availability. All the experimental data from this work is available online at Mendeley at http://doi.org/10.17632/ydw5kkzfjk.1.

ACKNOWLEDGMENTS. This work was supported by the National Natural Science Foundation of China (Nos. 42077193, 21906024, 91544224, 41775150, 41827804), the Shanghai Natural Science Foundation (No. 19ZR1404000), and the Excellence Initiative of Aix-Marseille University - A*MIDEX, a French "Investissements d'Avenir" programme - AMX-19-IET-010.

1. R. E. Cochran, O. S. Ryder, V. H. Grassian, K. A. Prather, Sea spray aerosol: The chemical link between the oceans, atmosphere, and climate. *Acc. Chem. Res.* **50**, 599–604 (2017).
2. D. C. Blanchard, The electrification of the atmosphere by particles from bubbles in the sea. *Prog. Oceanogr.* **1**, 73–202 (1963).
3. J. M. Michaud *et al.*, Taxon-specific aerosolization of bacteria and viruses in an experimental ocean-atmosphere mesocosm. *Nat. Commun.* **9**, 2017 (2018).
4. F. Veron, Ocean spray. *Annu. Rev. Fluid Mech.* **47**, 507–538 (2015).
5. A. H. Woodcock, C. F. Kientzler, A. B. Arons, D. C. Blanchard, Giant condensation nuclei from bursting bubbles. *Nature* **172**, 1144–1145 (1953).

6. D. E. Spiel, On the births of film drops from bubbles bursting on seawater surfaces. *J. Geophys. Res. Oceans* **103**, 24907–24918 (1998).
7. H. Lhuissier, E. Villermaux, Bursting bubble aerosols. *J. Fluid Mech.* **696**, 5–44 (2012).
8. E. R. Lewis, S. E. Schwartz, *Sea Salt Aerosol Production: Mechanisms, Methods, Measurements and Models - A Critical Review* (American Geophysical Union, Washington, DC, 2004).
9. K. A. Prather *et al.*, Bringing the ocean into the laboratory to probe the chemical complexity of sea spray aerosol. *Proc. Natl. Acad. Sci. U.S.A.* **110**, 7550–7555 (2013).
10. X. Wang *et al.*, Microbial control of sea spray aerosol composition: A tale of two blooms. *ACS Cent. Sci.* **1**, 124–131 (2015).
11. F. J. Resch, J. S. Darrozes, G. M. Afeti, Marine liquid aerosol production from bursting of air bubbles. *J. Geophys. Res. Oceans* **91**, 1019–1029 (1986).
12. D. C. Blanchard, A. H. Woodcock, Bubble formation and modification in the sea and its meteorological significance. *Tellus* **9**, 145–158 (1957).
13. X. Wang *et al.*, The role of jet and film drops in controlling the mixing state of submicron sea spray aerosol particles. *Proc. Natl. Acad. Sci. U.S.A.* **114**, 6978–6983 (2017).
14. J. Latham, M. H. Smith, Effect on global warming of wind-dependent aerosol generation at the ocean surface. *Nature* **347**, 372–373 (1990).
15. G. de Leeuw *et al.*, Production flux of sea spray aerosol. *Rev. Geophys.* **49**, RG2001 (2011).
16. D. Q. Pham *et al.*, Biological impacts on carbon speciation and morphology of sea spray aerosol. *ACS Earth Space Chem.* **1**, 551–561 (2017).
17. B. Stevens, G. Feingold, Untangling aerosol effects on clouds and precipitation in a buffered system. *Nature* **461**, 607–613 (2009).
18. Y. Wang, L. Bourouiba, Non-isolated drop impact on surfaces. *J. Fluid Mech.* **835**, 24–44 (2018).
19. W.-R. Ke, Y.-M. Kuo, C.-W. Lin, S.-H. Huang, C.-C. Chen, Characterization of aerosol emissions from single bubble bursting. *J. Aerosol Sci.* **109**, 1–12 (2017).
20. F. J. Blanco–Rodríguez, J. M. Gordillo, On the sea spray aerosol originated from bubble bursting jets. *J. Fluid Mech.* **886**, R2 (2020).
21. D. E. Spiel, The sizes of the jet drops produced by air bubbles bursting on sea- and fresh-water surfaces. *Tellus B Chem. Phys. Meterol.* **46**, 325–338 (1994).
22. K. Sellegri, C. D. O'Dowd, Y. J. Yoon, S. G. Jennings, G. de Leeuw, Surfactants and submicron sea spray generation. *J. Geophys. Res. Atmos.* **111**, D22215 (2006).
23. A. Berny, S. Popinet, T. Séon, L. Deike, Statistics of jet drop production. *Geophys. Res. Lett.* **48**, e2021GL092919 (2021).
24. C. F. Brasz *et al.*, Minimum size for the top jet drop from a bursting bubble. *Phys. Rev. Fluids* **3**, 074001 (2018).
25. A. M. Gañán-Calvo, Revision of bubble bursting: Universal scaling laws of top jet drop size and speed. *Phys. Rev. Lett.* **119**, 204502 (2017).
26. E. Ghabache, A. Antkowiak, C. Josserand, T. Séon, On the physics of fizziness: How bubble bursting controls droplets ejection. *Phys. Fluids* **26**, 121701 (2014).
27. J. M. Gordillo, J. Rodríguez-Rodríguez, Capillary waves control the ejection of bubble bursting jets. *J. Fluid Mech.* **867**, 556–571 (2019).
28. D. C. Blanchard, L. D. Syzdek, Film drop production as a function of bubble size. *J. Geophys. Res. Oceans* **93**, 3649–3654 (1988).
29. J. C. Bird, R. de Ruiter, L. Courbin, H. A. Stone, Daughter bubble cascades produced by folding of ruptured thin films. *Nature* **465**, 759–762 (2010).
30. G. Frens, Aerodynamic drag on bursting bubbles. *J. Phys. Chem.* **78**, 1949–1953 (1974).
31. H. Lhuissier, E. Villermaux, Soap films burst like flapping flags. *Phys. Rev. Lett.* **103**, 054501 (2009).
32. E. Villermaux, Fragmentation versus cohesion. *J. Fluid Mech.* **898**, 1 (2020).
33. F. Resch, G. Afeti, Submicron film drop production by bubbles in seawater. *J. Geophys. Res. Oceans* **97**, 3679–3683 (1992).
34. F. Resch, G. Afeti, Film drop distributions from bubbles bursting in seawater. *J. Geophys. Res. Oceans* **96**, 10681–10688 (1991).
35. G. B. Deane, M. D. Stokes, Scale dependence of bubble creation mechanisms in breaking waves. *Nature* **418**, 839–844 (2002).
36. P. K. Quinn *et al.*, Contribution of sea surface carbon pool to organic matter enrichment in sea spray aerosol. *Nat. Geosci.* **7**, 228–232 (2014).
37. S. M. Burrows *et al.*, A physically based framework for modeling the organic fractionation of sea spray aerosol from bubble film Langmuir equilibria. *Atmos. Chem. Phys.* **14**, 13601–13629 (2014).
38. R. E. Cochran, T. Jayarathne, E. A. Stone, V. H. Grassian, Selectivity across the interface: A test of surface activity in the composition of organic-enriched aerosols from bubble bursting. *J. Phys. Chem. Lett.* **7**, 1692–1696 (2016).
39. P. DeCarlo, J. Slowik, D. Worsnop, P. Davidovits, J. Jimenez, Particle morphology and density characterization by combined mobility and aerodynamic diameter measurements. Part 1: Theory. *Aerosol Sci. Technol.* **38**, 1185–1205 (2004).
40. Y. Toba, Drop production by bursting of air bubbles on the sea surface (II) Theoretical study on the shape of floating bubbles. *J. Oceanogr. Soc. Jpn* **15**, 121–130 (1959).
41. J. M. Thomas, X. Chen, A. Maißer, C. J. Hogan, Differential heat and mass transfer rate influences on the activation efficiency of laminar flow condensation particle counters. *Int. J. Heat Mass Transf.* **127**, 740–750 (2018).